Dynamic 3-D Virtual Fixtures for Minimally Invasive Beating Heart Procedures

Jing Ren, *Member, IEEE*, Rajni V. Patel, *Fellow, IEEE*, Kenneth A. McIsaac*, *Member, IEEE*, Gerard Guiraudon, and Terry M. Peters, *Senior Member, IEEE*

***Abstract*—Two-dimensional or 3-D visual guidance is often used for minimally invasive cardiac surgery and diagnosis. This visual guidance suffers from several drawbacks such as limited field of view, loss of signal from time to time, and in some cases, difficulty of interpretation. These limitations become more evident in beating-heart procedures when the surgeon has to perform a surgical procedure in the presence of heart motion. In this paper, we propose dynamic 3-D virtual fixtures (DVFs) to augment the visual guidance system with haptic feedback, to provide the surgeon with more helpful guidance by constraining the surgeon's hand motions thereby protecting sensitive structures. DVFs can be generated from preoperative dynamic magnetic resonance (MR) or computed tomograph (CT) images and then mapped to the patient during surgery. We have validated the feasibility of the proposed method on several simulated surgical tasks using a volunteer's cardiac image dataset. Validation results show that the integration of visual and haptic guidance can permit a user to perform surgical tasks more easily and with reduced error rate. We believe this is the first work presented in the field of virtual fixtures that explicitly considers heart motion.**

***Index Terms*—Beating heart surgery, dynamic virtual fixtures, haptic feedback, minimally invasive robot-assisted surgery.**

I. Introduction

CONVENTIONAL beating heart surgery has recently been extended to include robotic assistance to improve surgical dexterity [1]. Compared to the conventional open-chest arrested heart procedure, robot-assisted minimally invasive beating-heart surgery avoids the use of a sternotomy and a heart–lung machine. As a result, it provides patients with substantial benefits such as reduced trauma, shorter recovery time, and fewer complications. It also represents potential long-term fiscal savings for the health care system. While minimally invasive surgery (MIS) addresses many potential problems associated with conventional procedures, it nevertheless still suffers from several limitations, including restricted maneuverability and limited field-of-view, the surgical target is constantly in motion, and there is a lack of tactile feedback. These challenges raise critical issues with respect to surgical safety and precision. We believe that many of these issues can be addressed by the use of haptic virtual fixtures (VFs). VFs are computer-generated forces that are reflected back to the operator as feedback during a procedure. VFs can be placed in two categories: guidance virtual fixtures (GVFs), which can be used to guide the surgeon toward a target, and forbidden-region virtual fixtures (FRVFs), which restrict access to "forbidden" regions. GVFs can help an operator or robot to move along desired paths or organ surfaces, with the operator having the option to reject the guidance by applying additional force. On the other hand, FRVFs are hard constraints that aim to prevent the operator/robot from entering forbidden regions. As in the case of real fixtures, such as a ruler guiding a pencil, VFs still permit surgeons to retain ultimate control, but extend their capabilities, enhance the speed of surgery, and reduce mental stress by providing a local reference and restricting motion [2].

Since Rosenberg [3] implemented VFs for a "peg-in-hole" task in a teleoperated environment, renewed interest has been shown in their use for surgical guidance, in both teleoperated and cooperative systems. Among the work based on teleoperated systems, that of Park *et al.* [4] was the first reported attempt to transfer VFs to the operating room (OR). By using VFs generated from preoperative computed tomograph (CT) images, they constrained the motions of a Zeus robot (Computer Motion, Goleta, CA) to a predefined path during the dissection of the internal mammary artery (IMA). Prada *et al.* [5] applied VFs to cutting tasks during telemanipulation and training. Their study of the performance of these tasks in the presence of VFs suggests improvements in performance when force cues are provided to the operator. Using a potential field method, Turro *et al.* [6] implemented VFs on both the master and the slave sides of a teleoperated system. Work on developing VFs for cooperative systems has also been fruitful [2], [7], [10], with most of the research having been based on a "steady-hand" surgical robot [11]. Acrobot [12] and Cobot [13] are other types of

Manuscript received July 26, 2007; revised January 2, 2008. Published July 25, 2008 (projected). This work was supported in part by The Ontario Research and Development Challenge Fund (ORDCF) under Grant 00-May-0709, in part by the Ontario Consortium for Image-guided Therapy and Surgery (funded by ORDCF), in part by infrastructure grants from The Canada Foundation for Innovation awarded to The London Health Sciences Center (Canadian Surgical Technologies and Advanced Robotics), and in part by the Robarts Research Institute, and the National Science and Engineering Research Council (NSERC) of Canada under Grant RGPIN-1345, Grant RGPIN-249883, and Grant RGPIN-303802. *Asterisk indicates corresponding author.*

J. Ren is with University of Ontario Institute of Technology (UoIT), Oshawa, ON, L1H 7K4 Canada.

R. V. Patel is with the Department of Electrical and Computer Engineering, University of Western Ontario, London, ON,N6A 5B9 Canada and Canadian Surgical Technologies and Advanced Robotics, London, ON, N6A 5A5 Canada.

*K. A. McIsaac is with the Department of Electrical and Computer Engineering, University of Western Ontario, London, ON, N6A 5B9 Canada (e-mail: kmcisaac@engga.uwo.ca).

G. Guiraudon is with Canadian Surgical Technologies (CSTAR) and Advanced Robotics, London, ON, N6A 5A5 Canada.

T. M. Peters is with the Robarts Research Institute, London, ON, N6A 5K8 Canada.

Color versions of one or more of the figures in this paper are available online at http://ieeexplore.ieee.org.

Digital Object Identifier 10.1109/TMI.2008.917246

human/robot interaction devices, where the application of virtual fixtures is focused on constrained control algorithms operating on simple constraints. In these cases, online computation time is not always critical and speed is not a major concern. In this class of application, force is not always guaranteed to be continuous and the shape of force field cannot be easily adjusted online.

In the area of medical applications, VFs have generally been developed for simple tasks such as path following and obstacle avoidance, using simple lines or surfaces [2], [6]. However, to make VFs useful for surgical procedures, these fixtures need to consider more complex structures and be developed from patient-specific anatomy. Li *et al.* [7], [8] studied the tasks of path following and anatomic constraints for ENT surgery, and generated VFs directly from a patient's skull anatomy. However, they considered the task of controlling a robot and used covariance tree data structures to calculate anatomic constraints for the tool. The average computation time for one control loop is longer than that required to provide a stable haptic feedback (0.1–1 ms), therefore their method cannot be used directly to provide force cues to the surgeon side.

In this paper, we present an image and potential field-based VF generation method to render anatomical constraints sufficiently rapid to provide meaningful haptic feedback to the surgeon. To generate GVFs, we need to generate a potential field that has low potential values within a narrow range close to the preplanned path or surface, such as the heart surface and higher potential values when away from the path or surface. However to generate FRVFs, the whole protected area is treated as an obstacle and has high potential values. Since the generation of GVFs and FRVFs requires potential fields with different properties, we propose two types of field models: generalized sigmoid functions to generate FRVFs, and generalized Gaussian functions to generate GVFs. Both potential functions can accurately represent patient anatomy with real-time force reflection. The proposed VFs have several advantages such as computational efficiency, easily adjustable force reflection, and force continuity, allowing us to achieve the desired force reflection without unnecessarily reducing the surgical workspace.

In this work, we also consider the dynamic nature of the heart and develop dynamic virtual fixtures (DVFs) to accommodate the motion of the myocardium. DVFs can be applied to both GVFs and FRVFs. After VFs are built for each volume, and for all volumes in the preoperative dynamic magnetic resonance (MR) dataset, interpolation is performed to find a DVF at each time point over the cardiac cycle. As a result, we can constrain the operator's motion to the surface of a beating heart or to a prescribed region within a chamber. To the best of our knowledge, this work represents the first application of VFs to a dynamic anatomical surface.

The proposed dynamic virtual fixtures are applicable to many intracardiac procedures, including atrial-septal defect repair, valve repair and replacement, and ablation for atrial fibrillation, and have the potential to be used for robot-assisted procedures, and direct minimally invasive procedures, where the interaction tool is slaved to a haptic device.

As robust dynamic image registration techniques are incorporated into image-guidance for minimally-invasive procedures in general, they also become available to drive the construction of virtual fixtures for organs other than the heart. One could envisage for example the use of haptic constraints, based on virtual fixtures, to prevent the robot end-effector damaging sensitive tissues such as the neuro-vascular bundles during robotically-assisted prostate surgery.

One potential surgical application of DVFs is to help the surgeon during the treatment of Atrial Fibrillation (AF). A new approach described by Guiraudon *et al.* [9] proposes to introduce the ablation tool through the appendage of the left atrium, a procedure that provides increased control over the ablating instrument. It is envisaged that this procedure would ultimately be performed under robotic control and image-guidance provided by intracardiac echocardiography (ICE) or transesophageal echocardiogram (TEE) [9]. We believe that the introduction of VFs into this environment would further enhance the procedure by providing tactile cues to assist in the location of the ablation regions. Virtual fixtures can also help to constrain the surgical tool within the confined area, thus preventing accidental contact with sensitive tissue near the surgical site.

The rest of the paper is organized as follows. Section II presents some background on surgical guidance applications with application of VFs to a dynamic anatomical surface. Section III introduces an image-based implicitization method. Section IV presents the generation of FRVFs using generalized sigmoid functions and an application example, and Section V presents the generation of GVFs using generalized Gaussian functions, again with an application example. Section VI describes the application of DVFs for the beating heart. Section VII presents the registration of a haptic model to the patient. Section VIII summarizes the work and discusses some future research directions.

II. Surgical Guidance Methodology

Ongoing work in our lab aims to augment visual surgical guidance systems [14]–[16] with haptic feedback in order to complement the intraoperative environment that is designed to guide intervention based on preoperative MR and CT images, and intraoperative ultrasound (US) images. To achieve our goal, we need to perform the following discrete steps, which are represented in block diagram form in Fig. 1.

1) Acquire preoperative dynamic MR/CT images to construct a 3-D dynamic map of the surgical field.
2) Build VFs using MR/CT images and create a combined visual/haptic model.
3) Register this visual/haptic model to the patient in the operating room.
4) Acquire intraoperative US images with a tracked probe and map them to the integrated visual/haptic model to provide real-time force feedback to the surgeon during the surgical procedure.

All the preoperative preprocessing steps are performed prior to surgery, so the algorithms used in preprocessing steps are not time-critical. Conversely, the peri-operative and intraoperative algorithms are implemented in the operating room. In order that the haptics-augmented surgical guidance approach be accepted by surgeons, the steps being executed in the operating room must be optimized for speed.

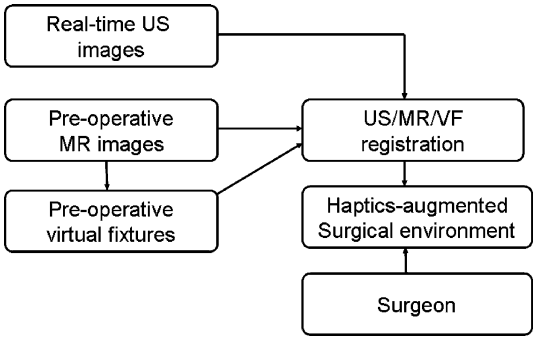

Fig. 1. Haptics-augmented image-guided minimally invasive surgery.

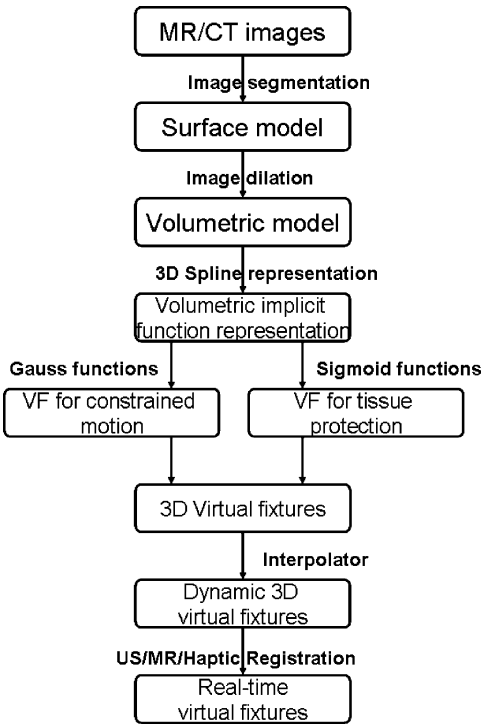

Fig. 2. Flowchart for generating dynamic 3-D VFs from preoperative MR/CT images.

The focus of this paper is on building DVFs from preoperative MR/CT images. Other elements in the haptics-augmented surgical guidance approach have been presented in other work, or are active research topics [16].

Fig. 2 presents an overview of the method. After a surface model is acquired through image segmentation, we create a volumetric model directly from the segmented MR/CT images (this technique is presented in Section III). The volumetric data are then used to train a spline neural network representation of the tissue shape, which in turn is used in our sigmoid function-based artificial potential field. Finally, the haptic model is mapped to ultrasound images to provide real-time force constraints.

III. Volumetric Implicit Function Generation

The image-based technique for volumetric implicit function generation consists of three steps: surface modeling, distance mapping using image dilation [17], and spline neural network training. We illustrate the technique working from an example of the heart extracted from MR images.

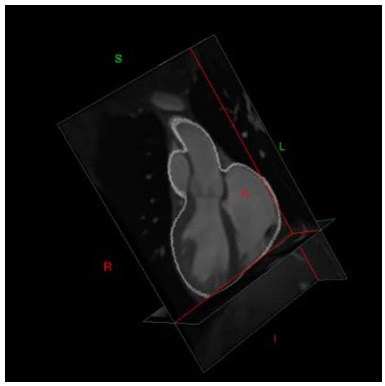

Fig. 3. MR dataset is segmented to create a surface model. Surface model is represented by the thin light-colored contour.

In the first step (see Fig. 3), a patient-specific model of the heart is created by segmenting the end-diastolic (ED) image of a 4-D dataset acquired with ECG-gating [15]. The modeling procedure begins with an acquisition of a 4-D dataset consisting of a set of several dynamic 3-D images depicting the subject's heart at different time points within the cardiac cycle. The end-diastolic (ED) frame from the 4-D dataset is chosen as the basis for the heart model. The chosen anatomy is then segmented in this image using a manual technique. The resulting binary segmentation image is then Gaussian filtered with a spherical kernel to smooth the edges. Finally, the marching cubes algorithm [15] is used to create a mesh of the segmented object. In the example heart model, there are 33 967 vertices and 90 700 triangles in the surface model.

The second step in the volumetric implicitization approach uses image dilation, to dilate the MR/CT surface data by one voxel at a time. After dilation, we can begin to build a *distance map*. It is known that each data point (identified by x, y, z coordinates) on the dilated image is one voxel away (in Euclidean distance) from the original surface map. The dilation process proceeds, and after each step, more data can be added to the distance map. Points found after two dilations are two voxels away from the tissue surface, points found after three dilations are three voxels away, and so on. This processing is continued until all of the voxels within the volume are distance-mapped. Fig. 4 illustrates one slice of the distance map.

In the work discussed in this paper, we used a spline neural network structure [18] based on B-spline basis functions to generate a smooth functional representation of the heart shape. Once the distance map is available and defined throughout the volume of interest, the spline neural network can be trained using this map data. The use of *B*-spline neural network functions was inspired by several attractive properties of *B*-splines and neural networks, including simplicity, generality, and local support. These properties make it particularly suitable to model our haptics-based system, which is a highly complex nonlinear function and requires rapid function evaluation and smooth scalar fields. Unlike typical *B*-spline approaches [19] that are only valid in the neighborhood of the surface, the spline neural network method used in this paper can define potential fields in

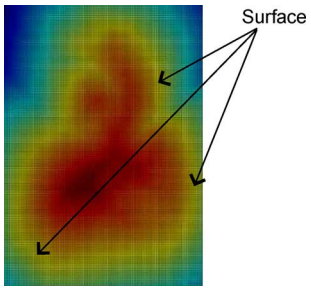

Fig. 4. This figure shows the signed distance map of the heart surface model generated by a morphological dilation operation. Distance value on the heart surface is zero (the brightest curve in the map). Signed distance value decreases further away from the center of the heart, with the color changing from warm to cold.

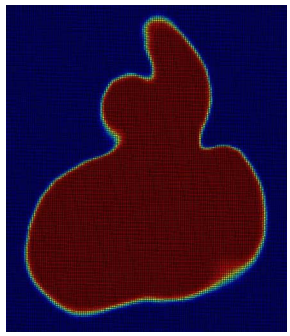

Fig. 5. This figure shows the potential fields of the distance map in Fig. 4 using the generalized sigmoid function. In this case, the potential field of the entire volume around (and including the interior) of the heart surface was generated. Note the fast transition from the value one (dark grey) on the inside to zero (black) on the outside.

the whole workspace, which is a more reasonable approach for surgical applications. The output is determined by

$$d(q) = d(x,y,z) = \sum_{i=0}^{l-1}\sum_{j=0}^{m-1}\sum_{k=0}^{n-1} p_{ijk} B_{i,r}(x) C_{j,s}(y) D_{k,t}(z) \tag{1}$$

where p_{ijk} are the weight parameters to be determined in the training process, $d(x,y,z)$ represents the distance value (determined in the distance map) at position $q = (x,y,z)$, $B_{i,r}(x)$, $C_{j,s}(y)$, and $D_{k,t}(z)$ are the basis functions corresponding to p_{ijk}, and l, m, n are dimensions of knot sequences in the x, y, z directions, respectively. r, s, t are the degrees of the basis functions $B_{i,r}(x)$, $C_{j,s}(y)$ and $D_{k,t}(z)$, respectively.

To train the spline neural network, we used the samples (q_n, d_n) in the distance map as pairs of points associated with distances from the tissue surface to solve for the weight parameters $p = \{p_{ijk}\}$ in the following optimization problem:

$$\min_p J = \frac{1}{N}\sum_{n=1}^{N}(f_{NN}(q_n,p) - d_n)^2 \tag{2}$$

where N is the number of training samples. Equation (2) is solved using the gradient approach defined by

$$p_{t+1} = p_t - \varepsilon \frac{\partial J}{\partial p} \tag{3}$$

where t is the iterative index, $\varepsilon > 0$ is the learning rate, $q_n = (x_n, y_n, z_n)$, and $f_{NN}(q_n,p) = d(x_n, y_n, z_n)$ is the output of the neural network.

Note that the initial parameters for the gradient optimization in (3) can be any randomly selected small values. Because the objective function in our formulation is of quadratic form, it has a unique global minimum that will always be found by the gradient descent method. After training, the time required at run time to compute the distance at any spatial point is invariant across datasets and patients due to the property of local support of the *B*-splines.

IV. Generating Forbidden-Region Virtual Fixtures Using Generalized Sigmoid Functions

In this section, we consider generating FRVFs to prevent the surgeon from accidentally damaging some delicate tissue, which in this paper is represented by the surface of the heart. A general potential field based on the generalized sigmoid function can be written as [20]

$$f(q) = f_{\text{sig}}(s) = \frac{1}{1+e^{-\gamma s}} \tag{4}$$

where we have introduced $s = d(q)$ as a distance function representing the distance from the object surface. The function s is defined so that on the boundary surface, $s = 0$, and all points on the boundary take a uniform potential value of 0.5. In the obstacle area, $s \gg 0$, and all points are associated with high potential values approaching unity. Outside the surface, $s \ll 0$, and potential values approach zero.

To illustrate the potential force model, we show in Fig. 5 the potential fields of one slice of a heart surface model. These fields are localized to the surface of the heart, and decrease sharply as we move farther away from the surface.

We define F'_q as the negative gradient of the potential field

$$F'_q = -\frac{\partial f(q)}{\partial q} = -\frac{\partial f_{\text{sig}}(d)}{\partial d}\frac{\partial d}{\partial q} \tag{5}$$

and the reflective force is

$$F_q = f(q)\frac{F'_q}{\|F'_q\|}. \tag{6}$$

As we illustrate in the next subsection, the use of generalized sigmoid functions provides the advantages of an easily adjusted protective area and continuous force feedback.

A. Evaluation I: Haptics-Guided Depth Control for Delicate Cutting Tasks

For all the experiments in this paper, we use the Freedom6S haptic device (MPB Inc., Montreal, QC, Canada) for haptic feedback. Because haptic feedback requires a much higher update rate ($\geq$ 1 kHz) compared to the 30 Hz update rate for the real-time graphics display, we use two threads of different priority. Both threads run on a Pentium IV computer (2.3 GHz) with 1 GB memory, which is equipped with the OpenGL/C++ graphics library, visualization toolkits (VTK) graphics library, and the C++ Freedom6S haptics library. The experimental configuration is shown in Fig. 6.

In this section, we consider a simulated cutting task. While cutting is common in most surgical procedures, it is more chal-

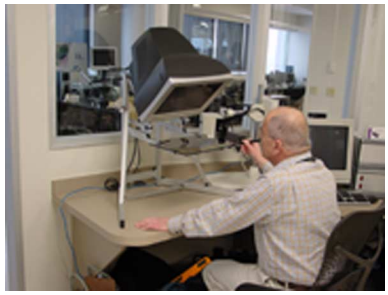

Fig. 6. Experimental configuration used for these experiments. Haptic device is manipulated while the user interacts with the virtual representation reflected in the half-silvered mirror. When stereoscopic visualization is employed, the user wears shuttered eye ware that admits successive left and right eye views to the appropriate eyes.

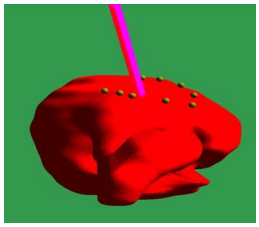

Fig. 7. This task simulates cutting by pushing the tool to the desired depth under the surface at select locations.

lenging in minimally invasive procedures because it is difficult to know how deep to make the cut, due to lack of force feedback. Our haptic force model can assist the operator in performing the optimal incision, by providing a perceived force feedback when the surgical instrument approaches the desired cutting depth. The use of the force model can enable cutting tasks to be performed safely and easily. To implement our approach, we generated a protective force field that closely surrounds the surface at the desired depth using the force model derived above. As the tool controlled by the user via the haptic interface approaches the desired depth, the user feels a force cue. The force experienced by the user increases as the user's tool approaches closer to the depth boundary, and decreases as the tool moves away. (While the force model is continuous and present everywhere in the simulated surgical field, it becomes imperceptible at some distance from the boundary). In this simulated cutting procedure shown in Fig. 7, we show a heart with ten "pellets." The pellets represent the preplanned cutting path. The goal of this procedure is to push the pellets into the heart but only to a specific level/depth. We use a probe with a tip as the "cutting tool." When the tip touches the center of the pellet, the cutting begins and the user starts to push. The pellet is released when the user believes it to be at the desired depth. The error between the actual and desired depths for each operation is then recorded and the root-mean-square (rms) error is calculated for ten pellets.

Six subjects from different groups (surgeon, scientist, research associate, and graduate students), representing users having varied experience with haptics, performed this procedure. The results of attempting to achieve a desired depth of 5 mm with the maximum force magnitude of 0.6 *N* are shown

TABLE I
PERFORMANCE EVALUATION (Mean $\pm$ std mm)

Subject	Depth with force (mm)	Depth without force (mm)
1	4.92±0.20	4.69±1.26
2	4.81±0.78	4.96±1.75
3	4.92±0.27	3.62±1.24
4	4.80±0.11	4.74±1.45
5	4.46±0.22	4.44±2.03
6	4.90±0.10	4.73±1.34

Six subjects attempted a 5mm deep cut with and without haptic guidance. The reduced standard deviation with force feedback illustrates the effectiveness of the method.

TABLE II
COMPUTATION TIME COMPARISONS

Method	Organ	Vertices	Triangles	Time
Co-variance tree	skull	99,000	182,000	32.4ms
Volumetric implicit	Heart	33,967	90,700	<0.2ms

in Table I. The depth recorded is the mean depth for all pellet insertions ($\sim$ 5 mm), and the reported SD is the variation of depth about this recorded mean throughout the procedure. Without haptic guidance, the users often overshot the targeted cutting depth. While the mean depth averaged over all trials and subjects was not significantly different for the two conditions, the variation was significantly different ($p < .001$). This result implies that, when employing a virtual fixture with a force of sufficient magnitude, the users can consistently cut close to the desired depth. While we allowed a training period for each subject to become familiar with the procedure, we found that training effects were minimal.

Compared with traditional methods of generating geometric constraints by searching through a set of triangles, our method needs much less online computation time. We have compared the computation times for generating geometric constraints involved in our method with those presented by Li and Taylor [7] and show the results in Table II. While our dataset has only half of the number of triangles compared to Li's dataset, our algorithm is over two orders of magnitude faster.

The accuracy of both Li's method and ours, largely depends on the fineness of the mesh. Therefore the accuracy for both methods should be similar provided that same mesh is used. To quantitatively evaluate the accuracy of our algorithm, we defined the points whose potential value equals 0.5 to be the new heart slice boundary after training. We then calculated the distance from the original surface to the trained surface. The mean distance between the two surfaces was 0.36 mm with standard deviation of 0.22 mm.

We also investigated the effects of different values of γ. The use of the generalized sigmoid function [(4)] allows us to control the degree to which the force field is localized. For large values of γ, we can generate a force field where strong forces exist only within an area very close to the protected tissue, and which decays very rapidly with distance. Small values of γ have the opposite effect and tend to enlarge the boundary of the protected zone, leading to more gradual force transitions. Fig. 8 illustrates

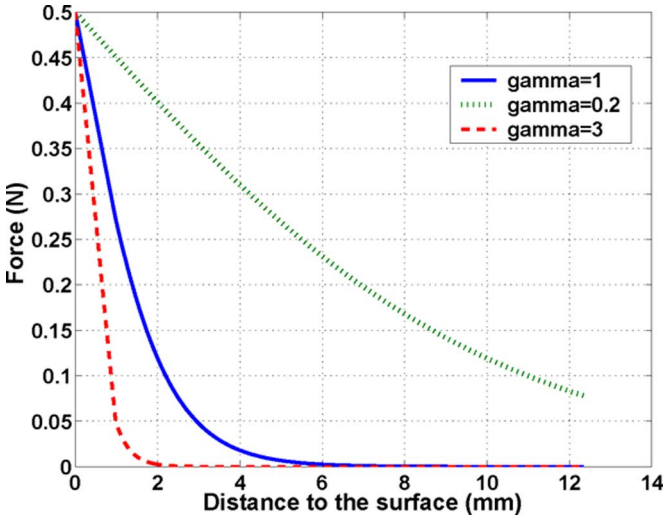

Fig. 8. Effect of γ (gamma) on force changes along with changing distance to the surface.

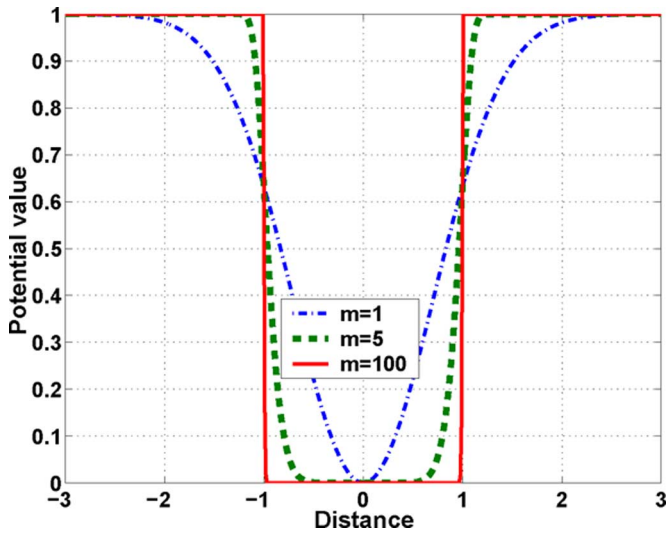

Fig. 9. In this figure, we show the effect of adjusting m. A large m can localize the force to the neighborhood of the boundary but may result in oscillation. A small m can achieve smooth force feedback but may restrict the surgeon's free motion in the surgery. An appropriate m can be determined experimentally.

the way in which the relationship between force and distance to the surface changes for different values of γ.

V. Generating Guidance Virtual Fixtures Using Generalized Gaussian Functions

In this section, we consider generating GVFs to constrain the surgeon's motion to a predefined region, in this case, the surface of the heart. The potential field based on generalized Gaussian functions can be written as [21]

$$f(q) = 1 - \exp\left(-\left(\frac{d(q)^2}{\delta^2}\right)^m\right) \tag{7}$$

where δ and m are adjustable parameters and can be easily determined experimentally.

Although continuity in the force model is helpful in eliminating undesired oscillations, the effect of an ideal virtual fixture should be imperceptible when the tool is within the desired region. Rather, the surgeon should only feel constraint forces when the tool is just about to stray outside the boundary of the desired zone.

In practice, this means that both the slope of the constraint forces through the boundary zone and the location of the boundary zone should be adjustable. By changing the slope, we can change the magnitude of the constraint force the surgeon feels as the tool approaches the boundary. By changing the location of the boundary zone, we can ensure that the desired region can be made as large as possible. In our formulation, both of these adjustments are possible through adjustments to the two parameters m and δ.

We show in Fig. 9 that the feedback force can be easily localized to the boundary of the confined region by adjusting the parameter m. In Fig. 9, distance 0 represents the surface. The planned workspace in this example was defined to be within 1 mm on each side of the surface, which is varied by adjusting δ. When we choose $m = 1$, it is clear that the operator will still perceive force even when the surgical tool is close to the surface. This condition can be improved by increasing m. However, an

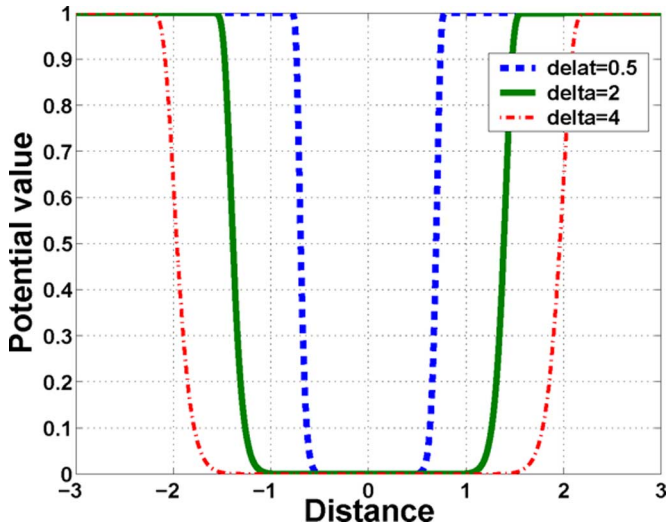

Fig. 10. In this figure, we show the effect of adjusting δ (delta). Value of δ determines the size of surgical space.

inappropriately large value of m may result in oscillations in the neighborhood of the boundary because its behavior approaches that of an on–off switch control.

The parameter δ can be used to adjust the size of the confined area. The goal of the GVFs is to ensure that the surgeon does not feel force if the motion of the surgical tool is within the desired area, while any attempts to leave this region are restricted. Fig. 10 demonstrates the adjustment of the size of workspace as a function of δ.

We define $F'_q(m)$ as the negative gradient of the potential field

$$F'_q(m) = -\frac{\partial f(q)}{\partial q}. \tag{8}$$

The force can be defined as

$$F_q = f(q)\frac{F'_q(m)}{||F'_q(m)||}. \tag{9}$$

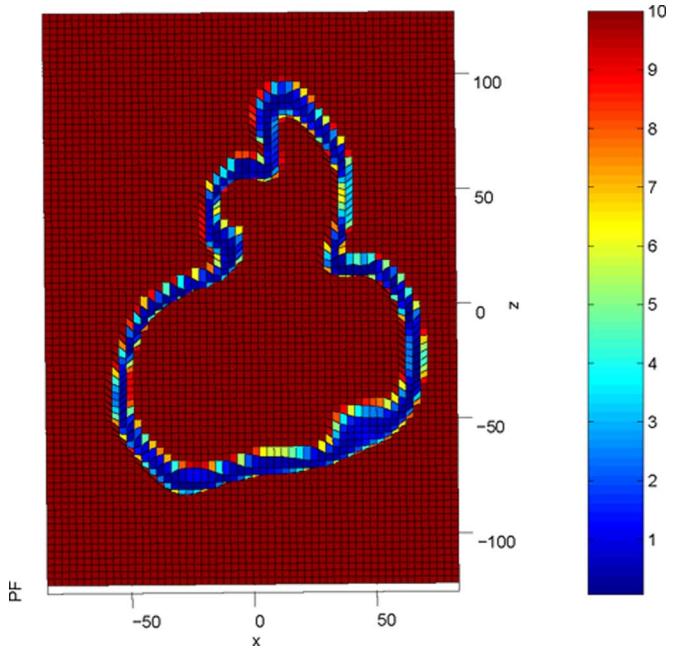

Fig. 11. This figure shows the potential fields of the distance map in Fig. 4 using the generalized Gaussian function.

To illustrate the potential force model, Fig. 11 shows the potential fields of one slice of a heart surface model. The potential fields take on zero values on the heart surface and increase as they move away from the surface.

A. *Evaluation II: Constrained Motion*

In the following experiment we applied haptic feedback, in a cooperative manner [7], [8] to a simulated conventional laparoscopic environment, where the haptic device is slaved to the laparoscope, and the hand is mapped to the proximal end of the laparoscopic probe, rather than the distal end as would be the case when using the daVinci robot. This introduces the additional challenge of hand–eye coordination that is present in all manual laparoscopic procedures. The proposed force models can also significantly enhance the performance of a robotic MIS system such as the da Vinci from Intuitive Surgical. Such a robotic MIS system provides good hand–eye coordination, high dexterity, and manipulability of surgical tools and high quality 3-D imaging. However, since surgical tools are inserted into the workspace through small incisions and surgeons operate with the aid of 3-D images provided by an endoscope also inserted through an incision, we believe that our proposed force models can significantly enhance the quality of image guidance in this case also.

Using generalized Gaussian functions, we can generate an attractive force around the target surface or line. When moving away from the predefined work area, the user feels a force pushing the hand back, making it easier to stay in the desired target area or path when the visual guidance is not sufficient. The force increases as the tool moves further away from the target, and conversely, it decreases as the tool moves back towards the target. The force model generates a fixture that is both continuous and soft; it is intended to provide guidance to the surgeon, rather than to restrict the motion of the instrument.

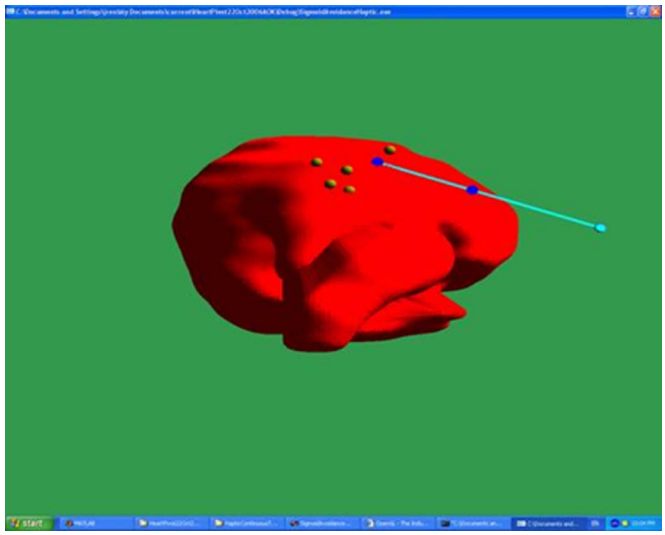

Fig. 12. Evaluation on a simulated tissue dissection task.

TABLE III
COMPARISONS OF TASK COMPLETION TIME (SECONDS)

Subject	T1	T2	T3	T4	T5	Mean
1	45	41	55	39	37	43±7
2	45	44	43	45	203	76±71
3	87	126	250	109	66	128±72
4	110	176	75	51	55	93±52
5	203	190	124	82	41	128±69
Grp Mean						94±64

(a)

Subject	T1	T2	T3	T4	T5	Mean
1	15	20	30	31	37	27±9
2	30	29	22	26	145	50±53
3	47	64	190	45	35	76±64
4	75	39	36	18	28	39±22
5	86	91	78	63	26	69±26
Grp Mean						42±41

(b)

In these tables, we show the comparison of the task completion time for 5 subjects performing the simulated dissection task (a) without and (b)with haptic feedback from the virtual fixture, using the configuration illustrated in Figure 6. Each row represents the task completion time in seconds for 5 trials (T1-T5) for each subject.

We performed a series of simulated tissue dissection experiments that employed a surgical tool passing through a fixed pivot point at the entry port on the patient surface. Fig. 12 illustrates a heart with ten pellets close to the surface. Each pellet represents a block of artificial tissue that needs to be removed from a location close to the heart. The goal of this procedure was to remove the tissue rapidly using a rod-like surgical tool. We generated a total of 100 pellets and five fulcrum points. For each run, a set of randomly selected pellets and a fulcrum point is used for evaluation to avoid the training effects. Each subject completed five trials with a different set of pellets and fulcrum for each trial.

Results from five subjects are shown in Table III. We observe that without haptic guidance, the users on average require almost 8 min to complete the entire task. However, when employing a virtual fixture, the users can remove all ten blocks of tissue in significantly less (55%) time ($p < .01$). As in the previous evaluation, the subjects are from different groups: surgeon, scientist, research associate, and graduate students. We

TABLE IV
MEAN TASK COMPLETION TIMES (SECONDS) WITH MONO AND STEREO DISPLAY

Subject	M-H	M-no-H	S-H	S-no-H
1	33.6	64.8	31.6	53.4
2	43.6	42.2	40.8	57.6
3	24.0	42.2	22.0	43.6
4	55.8	159.4	59.6	70.2
5	54.4	41.8	34.0	104
Means	42.3	71.3	37.6	67.6

In this table, we show the comparison of the mean time per trial in seconds for 5 subjects (S1-S5) to complete a series of simulated dissection tasks, similar to those reported in Table III, but this time with (H) and without (no H) haptic feedback, and with monoscopic (M) and stereoscopic (S) visualization.

did not observe significant differences among different groups, but found that people with experience with haptics can perform the experiments faster and with more accuracy, especially with force feedback. We also noticed that the users improve with training. To avoid training effects, each tester was given sufficient practice time before testing to allow them to reach a stable level of performance.

B. Performance Comparison With and Without a Stereoscopic Display

Robotically-assisted cardiac surgery is normally performed using a stereoscopic display of the surgical target. To investigate the influence of stereoscopic visualization on our methods, we tested the hypothesis that stereoscopic visualization would improve task execution time compared with the time taken using monoscopic visualization. Five operators were asked to perform a simulated cutting task, similar to that reported above, with and without haptic feedback, and with and without stereoscopic visualization. The results shown in Table IV illustrate that the mean task execution time approximately doubled when haptic guidance was removed. A student's t-test demonstrates that there is a significant difference ($p < .02$) between these two conditions. The test was then implemented using stereoscopic visualization to determine whether stereo cues were instrumental in improving the task results. In our experiment, the virtual heart model ($8 \times 8 \times 10$ cm) was placed in the plane of the viewing screen, 75 cm from the observers' eyes. Similar analysis of the results from the same five subjects performing the task showed no significant difference between the mean times taken with stereo enabled, compared to the times taken using monoscopic visualization. It is perhaps surprising that the use of stereo did not appear to improve the performance of this particular task, contradicting the observations of Drascic *et al.* [24]. However, as demonstrated by others [25], stereoscopic visualization does not always result in improved performance for surgical tasks. We conclude therefore that the advantage of stereo is task and environment specific.

VI. DYNAMIC 3-D VIRTUAL FIXTURES FOR THE BEATING HEART

It is important to model the motion of the heart because the large deformations can have a profound effect on accuracy of VFs, as well as the proper outcome for surgical planning and guidance. The animation of the beating heart volumes is based

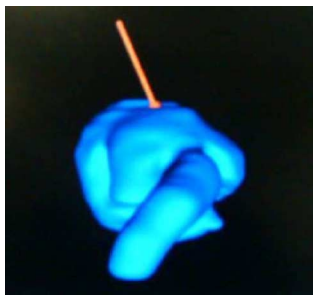

Fig. 13. Constrained motion using DVFs.

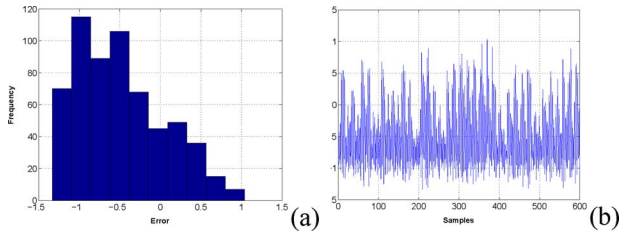

Fig. 14. Automatic tracking for 30 cardiac cycles. (a) Histogram of error distribution (in millimeters). (b) Measured sample errors.

on information contained in the series of 3-D images of the patient obtained over the cardiac cycle using ECG-gated imaging. Heart dynamics are extracted by studying the 3-D motion of the corresponding anatomy between the end-diastole (ED) frame and an earlier or later frame in the 4-D dataset, using an intensity based registration algorithm [15].

For this dynamic model, we used a guidance virtual fixture based on Gaussian potential fields. The procedure can be divided into two steps. First, a virtual fixture for each volume of the series of 3-D pre-operative heart images is created. These VFs are then linearly interpolated to generate a continuous real-time dynamic version.

If the current volume is V_i, the feedback force F can be calculated as follows:

$$F = \alpha F(V_i) + (1 - \alpha)F(V_{i+1}) \tag{10}$$

where $F(V_i)$ is the feedback force for the current volume V_i, $F(V_{i+1})$ is the feedback force for the next volume V_{i+1}, and α is given by

$$\alpha = \frac{t - t_i}{T_d} \tag{11}$$

where T_d is the display period of one volume (0.03 s/frame), t is the current time instant, t_i is the time instant to start displaying the current volume.

Fig. 13 shows that the tip of the surgical tool can be constrained to the surface of the beating heart using DVFs. The evaluations are performed for two cases: automatic tracking and manual tracking. In the first case, the tool is placed on the heart surface and the errors between the actual tip position and the heart surface are recorded. Fig. 14 shows the histogram of the error, as well as the raw data. The mean error is 0.29 mm in this example. In the second case, the users move the tool around while simultaneously attempting to keep the tool on the surface during the heartbeat, simulating a surgical procedure on the

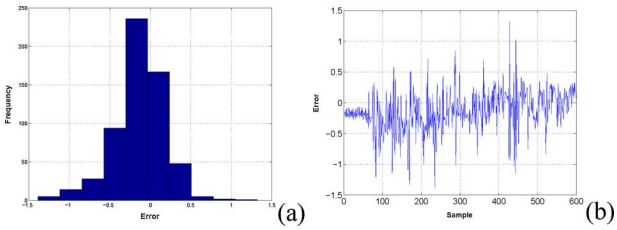

Fig. 15. Manual tracking for 30 cardiac cycles. (a) Histogram of error distribution (in millimeters). (a) Measured sample errors.

beating epicardial surface.The essential difference between the first and second examples is therefore is that the latter has the human in the feedback loop. Fig. 15 shows the error histogram and the raw data for the manual tracking case. Here, the mean error is 0.25 mm.

For this application, the preoperative data must have a sufficiently high temporal resolution to ensure that the interpolation provides a reasonable solution and to avoid aliasing. Smooth force feedback can be achieved with 20 volumes per cardiac cycle with linear interpolation between them. Although the cardiac motion is generally not linear in terms of tissue deformation, the largest motion of a point on the heart over one cardiac cycle in our model is ~ 5 mm, and the difference between two successive volumes is approximately 0.25 mm. Therefore, using a nonlinear interpolation is not expected to further improve the result.

Since all of this work has so far been performed in a simulated environment, we acknowledge that our validation procedure has its limitations. To properly assess the impact of virtual fixtures in a real-world application, we will in future integrate this work with both the operative system (daVinci) and cooperative assist devices, such as the John Hopkins "steady hand." As further discussed below, the accuracy of model to patient registration and instrument tracking is also critical to the success of this approach.

VII. Registration to Patient

It must be emphasized that, for this system to be effective, the model constructed from preoperative images must be robustly registered to the patient both spatially and temporally. In the cases when surgical deformation can be neglected and a high-frequency ventilator used to eliminate the deformation due to respiration, we can treat heart motion as pure periodic motion and use a rigid-body registration to align preoperative images and intraoperative US with the aid of ECG signals and tracking information from an US probe [16]. This rigid-body registration can then be used to update preoperative DVFs to match intraoperative images of the patient, as shown in Fig. 16. For the cases where heart deformation caused by surgery and/or surgical instruments cannot be ignored and the registration between preoperative images and intraoperative images is not a rigid mapping, registering virtual fixtures to the patient is not a trivial task. However, recent work in the cardiac image registration area [22], [23] has shown some promising progress in this direction.

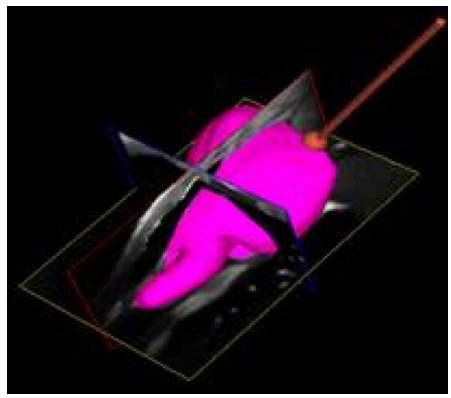

Fig. 16. In this figure, the haptic model is mapped to the patient dataset (US images) through US/MR image registration.

If the cardiac cycle is different only in heart rate and the motion pattern remains the same, we can adjust the display period T_d for one volume online to match virtual fixtures to the patient. However, if the cardiac behavior is abnormal and the motion pattern is totally changed, a nonrigid registration will inevitably be needed to warp virtual fixtures to the patient. This warping poses a challenging issue given the online computation power available.

VIII. Conclusion and Future Work

We have presented a method to augment a surgical guidance system with haptic feedback and to register the haptic model to the patient dataset. We have also described a method based on potential field methods for generating DVFs directly from preoperative MR/CT images, using a surface model based on a *B*-spline neural network. In our example, the haptic model was generated by a dynamic MRI-based model of the beating heart. Based on the results of our validations, we believe that this approach has great potential to significantly improve the safety and precision of robotically assisted image-guided surgery.

In the future, we will integrate this approach with other work in our laboratory and bring this method to clinical trial, which will allow us to evaluate the utility of a virtual fixtures model in a clinical environment. This method can also be used to assist surgical training and surgical planning. Specifically, we can identify different tissues in preoperative MR/CT images and generate haptic models using their material and surface properties such as softness, friction, and texture. In this manner, haptic feedback provides a complementary modality to visual feedback and can improve training and planning performance. By registering preoperative MR/CT with intraoperative US images, we can also map haptic properties of tissue onto tissues displayed in US images and perform training and planning with US images.

Acknowledgment

The authors would like to thank E. Huang, K. Wang, J. Moore, Dr. M. Wierzbicki, and C. Wedlake for their helpful contributions on various aspects of this project.

REFERENCES

[1] B. Kiaii *et al.*, "Minimally invasive endoscopic resection of a giant left atrial appendage aneurysm," *Ann. Thoracic Surg.*, vol. 77, pp. 1437–1438, 2004.

[2] A. Bettini, P. Marayong, S. Lang, A. M. Okamura, and G. D. Hager, "Vision-assisted control for manipulation using virtual fixtures," *IEEE Trans. Robot.*, vol. 20, no. 6, pp. 953–966, Dec. 2004.

[3] L. B. Rosenberg, "Virtual fixtures: Perceptual tools for telerobotic manipulation," in *IEEE Vitual Reality Int. Symp.*, Seattle, WA, 1993, pp. 76–82.

[4] S. Park, R. D. Howe, and D. F. Torchiana, "Virtual fixture for robotic cardiac surgery," in *Proc. 4th Int. Conf. Med. Image Comput., Comput. Assist. Intervention*, 2001, pp. 1419–1420.

[5] R. Prada and S. Payandeh, "A study on design and analysis of virtual fixtures for cutting in training environments," in *1st Joint Eurohaptics Conf. Symp. Haptic Interfaces Virtual Environ. Teleoperator Syst.*, 2001, pp. 1419–1420.

[6] N. Turro, O. Khatib, and E. Coste-Maniere, "Haptically augmented teleoperation," in *IEEE Int. Conf. Robotics Autom.*, Seoul, Korea, 2001, pp. 386–392.

[7] M. Li and R. H. Taylor, "Spatial motion constraints in medical robot using virtual fixtures generated by anatomy," in *IEEE Conf. Robotics Autom.*, New Orleans, LA, Apr./May 2004, pp. 1270–1275.

[8] M. Li, M. Ishii, and R. H. Taylor, "Spatial motion constraints using virtual fixtures generated by anatomy," *IEEE Trans. Robot.*, vol. 23, no. 1, pp. 4–29, Feb. 2007.

[9] G. M. Guiraudon *et al.*, "En bloc exclusion of the pulmonary vein region in the pig using off pump beating intra-cardiac surgery: A pilot study for mini-invasive surgery for atrial fibrilltion," *Ann. Thoracic Surg.*, vol. 80, pp. 1417–1423, 2005.

[10] P. Marayong and A. Okamura, "Speed-accuracy characteristics of human-machine cooperative manipulation using virtual fixtures with variable admittance," *Human Factors*, vol. 46, no. 3, pp. 518–532, 2004.

[11] R. H. Taylor, P. Jensen, L. Whitcomb, A. Barnes, R. Kumar, D. Stoianovici, P. Gupta, Z. Wang, E. deJuan, and L. Kavoussi, "A steady-hand robotic system for microsurgical augmentation," *Int. J. Robot. Res.*, vol. 18, no. 12, pp. 1201–1210, Dec. 1999.

[12] M. Jakopec, F. R. Baena, S. J. Harris, P. Gomes, J. Cobb, and B. L. Davies, "The hands-on orthopaedic robot "acrobot": Early clinical trials of total knee replacement surgery," *IEEE Trans. Robot. Autom.*, vol. 19, no. 5, pp. 902–911, Oct. 2003.

[13] C. A. Moore, J. Michael, A. Peshkin, and J. E. Colgate, "Cobot implementation of virtual paths and 3-D virtual surfaces," *IEEE Trans. Robot. Autom.*, vol. 23, no. 1, pp. 347–351, Feb. 2003.

[14] A. M. Chiu, D. Dey, M. Drangova, W. D. Boyd, and T. M. Peters, "3-D image guidance for minimally invasive robotic coronary artery bypass," *Heart Surg. Forum*, vol. 3, no. 3, pp. 224–231, 2000.

[15] M. Wierzbicki, M. Drangova, G. Guiraudon, and T. M. Peters, "Validation of dynamic heart models obtained using nonlinear registration for virtual reality training, planning, and guidance of minimally invasive cardiac surgeries," *Med. Image Anal.*, vol. 8, no. 3, pp. 387–401, 2004.

[16] X. Huang, N. A. Hill, J. Ren, G. Guiraudon, D. Boughner, and T. M. Peters, "Dynamic 3-D ultrasound and MRI image registration of the beating heart," in *Med. Imag. Comput. Computer-Assisted Intervention (MICCAI)*, 2005, vol. 3750, pp. 171–178.

[17] E. R. Dougherty and R. A. Lotufo, *Hands-on Morphological Image Processing*. Bellingham, WA: SPIE Press, 2003.

[18] A. Cretu, E. M. Petriu, and G. G. Patry, "Neural network architecture for 3-D object representation," in *Proc. IEEE Int. Workshop Haptic, Audio Visual Environ. Appl.*, Ottawa, ON, Canada, 2003, pp. 31–36.

[19] J. Hua and H. Qin, "Haptic-based dynamic implicit solid modeling," *IEEE Trans. Vis. Comput. Graph.*, vol. 10, no. 5, pp. 574–586, Sep./Oct. 2004.

[20] J. Ren, K. A. McIsaac, and R. V. Patel, "A potential model using generalized sigmoid functions," *IEEE Trans. Syst. Man Cybern. B*, vol. 37, no. 2, pp. 477–484, Apr. 2007.

[21] J. Ren and K. A. McIsaac, "A hybrid-systems approach to potential field navigation for a multi-robot team," in *Proc. IEEE Int Conf. Robot. Autom.*, Sep. 2003, vol. 3, pp. 3875–3880.

[22] S. Szpala, M. Wierzbicki, G. Guiraudon, and T. M. Peters, "Real-time fusion of endoscopic view with dynamic 3-D cardiac images: A phantom study," *IEEE Trans. Med. Imag.*, vol. 24, no. 9, pp. 1207–1215, Sep. 2005.

[23] G.-A. Turgeon, G. Lehmann, G. Guiraudon, M. Drangova, D. Holdsworth, and T. M. Peters, "2D-3-D registration of coronary angiograms for cardiac procedure planning and guidance," *Med. Phys.*, vol. 32, no. 12, pp. 3737–3749, 2005.

[24] D. Drascic, P. Milgram, and J. J. Grodski, "Learning effects in telemanipulation with monoscopic versus stereoscopic remote viewing," presented at the IEEE Int. Conf. Syst., Man, Cybern., Boston, MA, 1989.

[25] M. Wentink, J. J. Jakimowicz, L. M. Vos, D. W. Meijer, and P. A. Wieringa, "Quantitative evaluation of three advanced laparoscopic viewing technologies: A stereo endoscope, an image projection display, and a TFT display," *Surgical Endoscopy*, vol. 16, no. 8, pp. 1237–1241, Aug. 2002.